

Exact Normal Modes of Quantum Plasmas

Tian-Xing Hu,¹ Dong Wu,^{1, a)} Z. M. Sheng,² and J. Zhang^{1,3, b)}

¹⁾Key Laboratory for Laser Plasmas and School of Physics and Astronomy, and Collaborative Innovation Center of IFSA, Shanghai Jiao Tong University, Shanghai, 200240, China

²⁾Institute for Fusion Theory and Simulation, Department of Physics, Zhejiang University, Hangzhou 310027, China.

³⁾Institute of Physics, Chinese Academy of Sciences, Beijing 100190, China.

The normal modes, i.e., the eigen solutions to the dispersion relation equation, are the most fundamental properties of a plasma, which also of key importance to many nonlinear effects such as parametric and two-plasmon decay, and Raman scattering. The real part indicates the intrinsic oscillation frequency while the imaginary part the Landau damping rate. In most of the literatures, the normal modes of quantum plasmas are obtained by means of small damping approximation (SDA), which is invalid for high- k modes. In this paper, we solve the exact dispersion relations via the analytical continuation (AC) scheme, and, due to the multi-value nature of the Fermi-Dirac distribution, reformation of the complex Riemann surface is required. It is found that the change of the topological shape of the root locus in quantum plasmas is quite different from classical plasmas, in which both real and imaginary frequencies of high- k modes increase with k in a steeper way than the typical linear behaviour as appears in classical plasmas. As a result, the temporal evolution of a high- k perturbation in quantum plasmas is dominated by the ballistic modes.

I. INTRODUCTION

The study of quantum plasmas has important applications in the fields of, e.g., astrophysics¹, nano-physics^{2,3}, warm dense matter⁴, and inertial confinement fusion⁵⁻⁷, and thus received widespread attention in recent years. However, some of its fundamental properties have rarely been seriously discussed. For example, the exact eigen solution of a degenerate quantum plasma. In this paper, we solve the Landau damping rate by means of analytical continuation (AC) method, and avoid the branch cut discontinuity by extending the Riemann surface of the 1d Fermi-Dirac distribution function (1dFDDF). The AC method is a crucial step to comprehend the damping normal modes of plasmas, proposed by Landau a long time ago, which is widely used in the field of classical plasmas, but rarely discussed for quantum plasmas. The AC method is able to solve the exact normal modes with arbitrarily high wave numbers, which are important when micro-scale quantum kinetic effects are involved. And, the exact linear dispersion relation of real frequency helps us better understand nonlinear phenomena, namely, the coupling between different linear modes, and the exact imaginary frequency determines the lifetime of a plasmon.

The theoretical basis of this paper is the so-called collisionless quantum kinetic theory (QKT), which is, mathematically speaking, a Wigner-Poisson system (WPS) of equations. The linearized WPS is equivalent to the famous Random Phase Approximation (RPA), or the time-dependent Hartree approximation, which is well-proved to be a very successful model for quantum plasmas when the density is higher than the typical solid density ($\sim 10^{24}\text{cm}^{-3}$). Such a dense, degenerate electron environment is ubiquitous in the universe. For example, the core of the sun is partially degenerate, the core

of a white dwarf is extremely degenerate, and, the progenitors of most of energetic astrophysics events such as X-/ γ -ray burst and supernova explosion, are assumed to be related to extreme environments^{8,9}. In laboratories, some of the inertial confinement fusion experiment also produce degenerate quantum plasmas, e.g., the double-cone ignition⁵ (DCI) scheme. Hence, this work may has a wide range of applications.

This paper is organized as follow. In Sec. II, we introduced the complex structure of the Fermi-Dirac distribution function, then briefly reviewed the collisionless QKT and the corresponding linear response theory, which is the theoretical basis of this paper. In Sec. III, we discussed the complex structure of the dielectric function of quantum plasmas. And thus the exact linear dispersion relation of quantum Langmuir wave is solved by means of the aforementioned methods. Numerical simulations are also presented to verify the results. Further discussion and main conclusion are presented in Sec. IV.

II. THEORIES AND METHODS

We define a quantum parameter

$$\hat{\hbar} \equiv \frac{\hbar\omega_p}{2E_F}, \quad (1)$$

sometime is referred to as the normalized Planck's constant. Here, $\omega_p = \sqrt{4\pi e^2 n/m_e}$ is the plasma frequency, and the Fermi energy $E_F = \hbar^2(3\pi^2 n)/2m_e$. It seems strange that $\hat{\hbar}$ is proportional to $n^{-1/2}$, since we expect that quantum effects should be stronger for higher density. However, quantum effects are also stronger for lower temperature, while $\hat{\hbar}$ solely dependent on n . Hence, to measure the importance of quantum wave effects, a more appropriate choice would be

$$\tilde{\hbar} \equiv \frac{\hbar\omega_p}{2k_B T}, \quad (2)$$

^{a)}Electronic mail: dwu.phys@sjtu.edu.cn

^{b)}Electronic mail: jzhang1@sjtu.edu.cn

and once the degeneracy $\Theta = k_B T / E_F$ (the inverse of which measures the importance degeneracy) is fixed, decreasing \hbar means increasing $\tilde{\hbar}$.

In this paper, we adopt the natural unit system, where $\hbar = m_e = e = k_B = 1$. And the frequency, number density, velocity, length, and energy, are normalized to ω_p , n_e (electron density), v_F (Fermi velocity), $\lambda_F = v_F / \omega_p$, and E_F respectively.

A. Analytical structure of the 1dFDDF

The equilibrium state of electron obeys the 3d Fermi-Dirac distribution (3dFDDF)

$$\begin{aligned} f_{3d}(\mathbf{v}) &= \frac{3}{4\pi} \frac{1}{e^{(v^2 - \mu)/\Theta} + 1} \\ &= -\frac{3}{4\pi} \text{Li}_0 \left[-e^{(\mu - v^2)/\Theta} \right], \end{aligned} \quad (3)$$

where Li_n is the n -th order polylogarithm, and the value of the chemical potential $\mu = \mu(\Theta)$ is chosen such that $\int f_{3d}(\mathbf{v}) d^3v = 1$.

As a fundamental study, we only consider the interaction of electrons to a plane wave field, hence we can integrate over the dimensions perpendicular to the wave, namely, we only care about the 1d Fermi-Dirac distribution (1dFDDF) $f_{1d}(v_{\parallel}) = \iint d\mathbf{v}_{\perp} f_{3d}(v_{\parallel}, \mathbf{v}_{\perp})$. It is easy to prove that,

$$\begin{aligned} f_{1d}(v) &= -\frac{3}{4} \Theta \text{Li}_{\frac{1}{2}} \left[-e^{(\mu - v^2)/\Theta} \right] \\ &= \frac{3}{4} \Theta \ln \left[e^{(\mu - v^2)/\Theta} + 1 \right]. \end{aligned} \quad (4)$$

Let v be a complex variant $v = v_r + iv_i$, then the 1dFDDF is a multi-value function, the branch cuts of which are

$$v_r v_i = \pm \frac{\pi}{2} \ell \Theta, \quad \ell \in 2\mathbb{Z}, \quad (5)$$

and the branch points are located at the hyperbola:

$$v_r^2 - v_i^2 = \mu. \quad (6)$$

The structure of the 1dFDDF is also thoroughly discussed in Ref. 10. The density of the branch points on the hyperbola increases with decreasing Θ . In Fig. 1, we plotted the 1dFDDF in complex- v plane, one can see that its imaginary part is discontinued at the branch cuts. These discontinuities are equal to the height of a Riemann leaf, which is $3\pi\Theta/2$ here, and they exist because we considered only a single leaf the Riemann surface, see Fig. 2 (a). However, the Riemann surface of 1dFDDF has an infinite leaves because of the logarithm in Eq. (4), see Fig. 2 (b). Discontinuity may cause unphysical effects, as we shall see in the next subsection. Hence, we extend the area enclosed by the first branch cut and the hyperbola to the whole Riemann surface, as is shown in Fig. 2 (c), we then obtain a smooth surface between the two branches of the hyperbola. Noticing that, after this operation, the discontinuities do not vanish, but are moved from the branch cuts to the hyperbola.

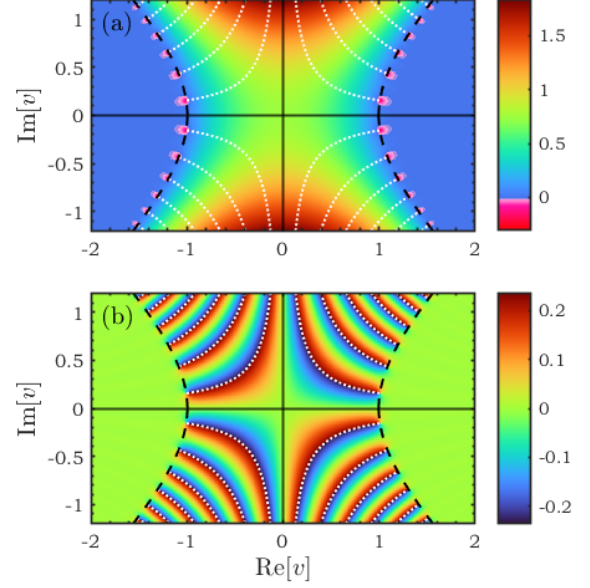


Figure 1. (a) Real (b) Imaginary part of the 1dFDDF ($\Theta = 0.1$). The dash-lines are the hyperbolae of Eq. (6), and the white dotted-lines are the branch cuts of Eq. (5).

B. The Linearized WPS

The electrons in a collisionless quantum plasma obey the Wigner equation¹¹

$$\partial_t f + \mathbf{v} \cdot \partial_{\mathbf{x}} f + i \vartheta_{i\hbar\partial_{\mathbf{p}}} [\phi(\mathbf{x})] f = 0. \quad (7)$$

Here $f = f(\mathbf{x}, \mathbf{v}, t)$ is the Wigner quasi-distribution function, which is the quantum counter part of the classical distribution function, and the pseudo-differential operator ϑ is defined by

$$\vartheta_{\mathbf{y}}[O(\mathbf{x})] \equiv O\left(\mathbf{x} + \frac{\mathbf{y}}{2}\right) - O\left(\mathbf{x} - \frac{\mathbf{y}}{2}\right). \quad (8)$$

Noticing that when $y \ll x$, $\vartheta_{\mathbf{y}}[O(\mathbf{x})] \simeq \mathbf{y} \cdot \nabla O$, then Eq. (7) reduces to the Vlasov equation, thus the Wigner equation is also called the quantum Vlasov equation.

And we need the Poisson equation

$$-\nabla^2 \phi = n_b - e \int f d\mathbf{v}, \quad (9)$$

where n_b stands for the background ion density, to close the system. Let $f = f_0 + \delta f$, $\phi = \phi_0 + \delta \phi$, and consider only the direction parallel to the wave vector, the linear evolution of the perturbed field can be formally written as¹²

$$\delta \phi(t, k) = \frac{i}{k^2} \iint d\mathbf{v}_{\parallel} \frac{d\omega}{2\pi} \frac{\delta f_{k0}(v_{\parallel}) e^{-i\omega t}}{(\omega - kv_{\parallel}) \varepsilon(\omega, k)}, \quad (10)$$

where $\delta f_{k0}(v)$ is the initial perturbation, and the dielectric function (DF) is defined as

$$\varepsilon(\omega, k) = 1 + \frac{1}{k^2} \mathcal{W}(\hbar\omega, \hbar k), \quad (11)$$

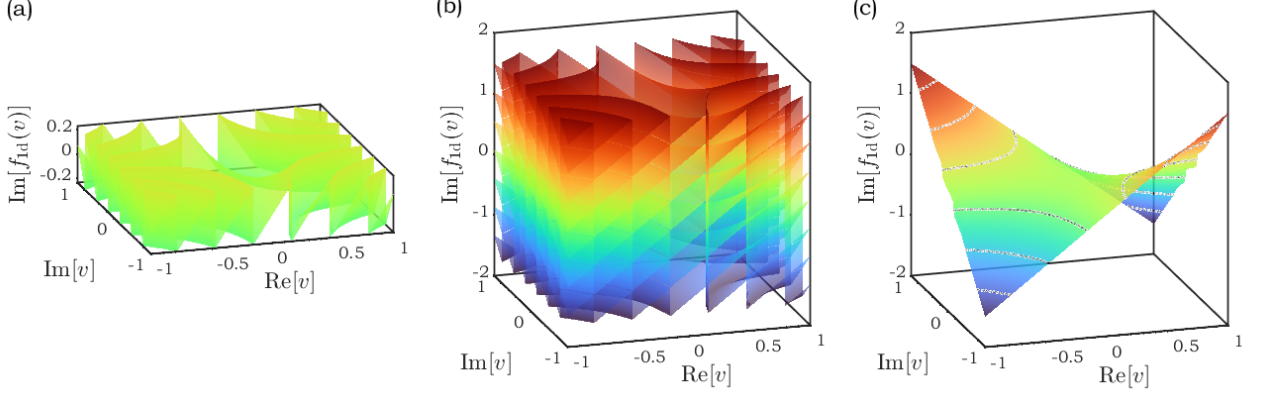


Figure 2. (a) A single leaf (b) Seven leaves (c) Extended single leaf of the 1dFDDF ($\Theta = 0.1$) Riemann surface.

where

$$\mathcal{W}(\omega, k) = \int dv \frac{\partial_k [f(v)]}{\omega - kv} \quad (12)$$

is the Lindhard response function¹³ (LRF). As $\Theta \rightarrow \infty$, $f(v)$ tends to Maxwellian, namely, in the classical limit, it reduces to

$$\mathcal{W}(\omega, k) = \frac{2}{\Theta} \frac{1}{\sqrt{2\pi}} \int dv \frac{ve^{-\frac{v^2}{2}}}{v - \omega/k_\Theta} = -\frac{2}{\Theta} Z' \left(\frac{\omega}{k_\Theta} \right), \quad (13)$$

where $k_\Theta = k\sqrt{\Theta/2}$, and Z is the famous plasma dispersion function. It is evident that in quantum plasma, the linear response is dependent on both ω and k , but in classical plasma, it depends only on the ratio of ω to k . The response function then does not depend on $\hat{\hbar}$, which means that when Θ is large enough, the system naturally returns to classical, no matter the value of $\hat{\hbar}$.

The roots of the eigen-equation

$$\varepsilon(\omega, k) = 0 \quad (14)$$

yield the dispersion relation of the normal modes. Here, $\omega = \omega_r + i\omega_i$ is a complex number. To calculate the DF (11) exactly with negative value of ω_i and solve Eq. (14), analytical continuation (AC) is needed for $\omega_r = 0$ is a branch cut, namely, when $\omega_i < 0$, the response function (12) should be modified to

$$\mathcal{W}(\omega, k) = \int dv \frac{\partial_k [f(v)]}{\omega - kv} - 2\pi i \partial_k \left[f \left(\frac{\omega}{k} \right) \right], \quad (15)$$

where the $2\pi i$ term stems from the residue of the integrand of Eq. (12). In the classical limit, it is

$$\frac{\Theta}{2} \mathcal{W}(\eta) = 1 - \sqrt{2} \eta F \left(\frac{\eta}{\sqrt{2}} \right) + i \sqrt{\frac{\pi}{2}} \eta e^{-\frac{\eta^2}{2}}, \quad (16)$$

where $\eta = \omega/k_\Theta$, and

$$F(x) = e^{-x^2} \int_0^x e^{t^2} dt \quad (17)$$

is the Dawson integral.

III. QUANTUM LANGMUIR WAVE

A. Solving the Normal Modes

The Landau damping rate is the negative imaginary part of the eigen-frequency. To calculation the DF with negative imaginary frequency, analytical continuation is needed. Noticing that for extremely degenerate plasmas, analytical continuation is not needed when $k < k_F = v_F = \omega_p \lambda_F^{-1}$, since the dielectric function has an analytic solution when $\Theta \rightarrow 0$:

$$\text{Re}[\varepsilon] = 1 + \frac{3}{2k^2} \left[1 + \frac{1}{2\hat{\hbar}k} (1 - b_-^2) \ln \left| \frac{1 + b_-}{1 - b_-} \right| - \frac{1}{2\hat{\hbar}k} (1 - b_+^2) \ln \left| \frac{1 + b_+}{1 - b_+} \right| \right], \quad (18)$$

$$\text{Im}[\varepsilon] = \frac{3\pi^2}{4\hat{\hbar}k^3} \ln \frac{1 + \exp[(b_+^2 - \mu)/\Theta]}{1 + \exp[(b_-^2 - \mu)/\Theta]}, \quad (19)$$

where

$$b_\pm = \frac{\omega}{k} \pm \frac{\hat{\hbar}k}{2}. \quad (20)$$

Thus one can see than only when $|b_\pm| > 1$, namely,

$$-k \pm \frac{\hat{\hbar}k^2}{2} < \omega < k \pm \frac{\hat{\hbar}k^2}{2}, \quad (21)$$

the DF has finite imaginary part. The area enclosed by (21) is referred as to the electron-hole excitation continuum (EHEC), in which a plasmon delay into an electron and a hole. The above formula is obtained based on the small damping approximation (SDA):

$$\lim_{y \rightarrow 0} \frac{1}{x \pm iy} = \mathcal{P} \frac{1}{x} \mp i\pi \delta(x), \quad (22)$$

which is incorrect when ω_i is finite. In the following, we directly solve the Eq. (15) without any approximation scheme.

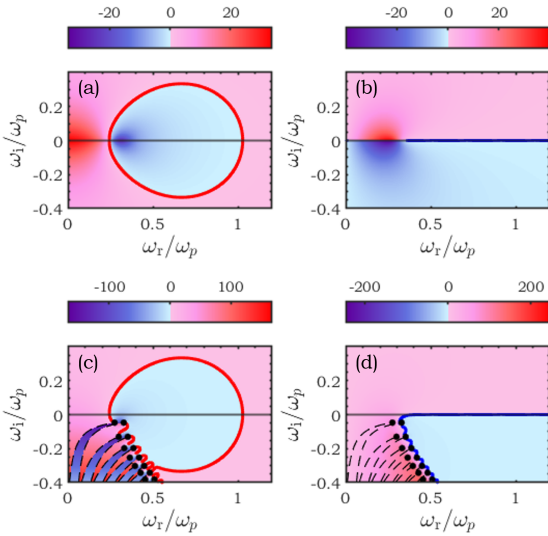


Figure 3. (a) (b): Real and imaginary part of the dispersion function without analytical continuation, and (c) (d): with analytical continuation. The dashed-lines are mappings of the branch cuts. The red lines stand for $\text{Re}[\varepsilon(\omega, k)] = 0$, and blue lines for $\text{Im}[\varepsilon(\omega, k)] = 0$.

In Fig. 3, the numerical results of dispersion function with or without AC are presented ($\Theta = 0.1, \hat{\hbar} = 0.6$), where the wave number $k = 0.3$. The upper two panels (a) and (b) are the real and imaginary parts of the DF without AC, while the lower two are with. It is shown that the discontinuity of the 1DFDDF is explicitly mapped from the complex ν plane to the complex ω plane by the \mathcal{D} operator, since in the calculation, we used the non-extended 1DFDDF, i. e., the single leaf Riemann surface of Fig. 2 (a). The series of pairs of black dots in the lower half plane are located at two hyperbolas, whose vertices are $\mu k \pm \hat{\hbar} k^2/2$ respectively.

In the rest of this paper, the imaginary part of the DF would not be presented, but we still keep the $\text{Im}[\varepsilon(\omega, k)] = 0$ lines in the real DF diagrams. And the colorbar will also be neglected since the absolute values of the DF are irrelevant in the context.

Take an example of a degenerate plasma, say, with density $n = 3 \times 10^{26} \text{cm}^{-3}$, and temperature $T = 300 \text{eV}$. Then we have the quantum parameter $\hat{\hbar} = 0.2$ and $\Theta = 0.2$. The real DF of such parameters in complex frequency plane are plotted In Fig. 4, where the real root loci are indicated by red lines and the imaginary loci by blue lines. Noticing that the real and imaginary loci have multiple intersections, which stand for multiple solutions of the normal modes. Generally, we only care about the least damping mode, i.e., the intersection point with maximum ω_i , which we indicated by black crosses in Fig. 4 and labeled its value. In panels (a) to (e), we used the single leaf 1DFDDF, the discontinuities occur at the branch cuts. One can see that there are no intersections in panel (e), so we have to use the extended 1DFDDF to move the discontinuities to the hyperbolas, as is seen in panel (f), in which a damping mode is obtained.

For another example of extremely degenerate plasma, we choose density $n = 3 \times 10^{29} \text{cm}^{-3}$, and temperature $T = 10^3 \text{eV}$, which could be the interior of a typical small white dwarf. Then we have the $\hat{\hbar} = 0.06$ and $\Theta = 0.005$. The DF results are presented in Fig. 5. One finds that, at such small Θ , the distance among each branch cuts are extremely small. All the modes with finite damping rate are located between the two hyperbolas (a gap opened by quantum wave effect). Hence the extend 1DFDDF is indispensable in this case. From Fig. 5, one also finds that when ω_i is finite,

$$\omega_r \simeq \mu k + \frac{\hat{\hbar} k^2}{2}, \quad (23)$$

and since $\mu \rightarrow 1$ when $\Theta \rightarrow 0$, this is upper bound of the EHEC.

Now we briefly discuss the topological features of the root loci. Generally, the imaginary locus starting from $\infty + 0i$, passing through every pair of branch point, while the real locus starting from one of the branch points and end with another. If the starting and ending points are a pair, and the locus is above the line joining the two branch points, we refer to this topological shape as “classical”, for it is topologically identical to the classical solution, see Fig. 6 (The classical thumb-like figure is very common in the field of classical plasma instabilities, e.g., see Ref. 14). Otherwise it is a “quantum” shape. For example, the (a) ~ (d) panels in Fig. 4 are classical, while (d), (e) and (f) are quantum. And in extremely degenerate case like Fig. 5, the classical shape does not exist at all. Furthermore, a quantum shape means that the least damping mode is most likely located within the two hyperbolas.

In Fig. 6, the classical sub-figure is calculated via Eq. (16), and the other two are quantum results with $\Theta = 4$, which is almost Maxwellian, it is shown that the normal modes in these there sub-figure are fairly close to one another. As $\Theta \rightarrow \infty$, all the branch points going to $-i\infty$, and we know that the value of $\hat{\hbar}$ (or $\tilde{\hbar}$) only effects the distance between a pair of branch points. This diagrammatically demonstrated that the larger Θ is, the less important the value of $\hat{\hbar}$ (or $\tilde{\hbar}$) is.

B. Exact Solution of the Normal Modes

It is worth mentioning that, $\varepsilon(\omega, k) = 0$ has multiple roots in a finite region of the complex ω plane, as one can see from Fig. 3, but we only care about the lowest damping mode. Hence, to solve the full dispersion relation of the QWL, we can starting from $k \simeq 0^+$, and calculate a small region centered at $\omega_0 = 1 + 0^+i$ to find the first root ω_1 and record the difference $\Delta\omega_1 = \omega_1 - \omega_0$. Then increasing k with a small value and calculating a next region centered at $\omega_1 + \Delta\omega_1$ to find the second root. Repeating this procedure, then a continuous curve of the complex frequency of the QWL as a function of k is obtained. The full solutions of normal modes $\omega(k)$ with different densities are plotted in Fig. 7. In panel (a), where $\hat{\hbar} = 0.4$ is corresponding to electron number density $n = 4 \times 10^{24} \text{cm}^{-3}$, and $\Theta = 0.2, 0.4$, and 0.8 , are corresponding to the temperature $T = 19, 37$ and 74eV . In panel (b), where $\hat{\hbar} = 0.2$ is

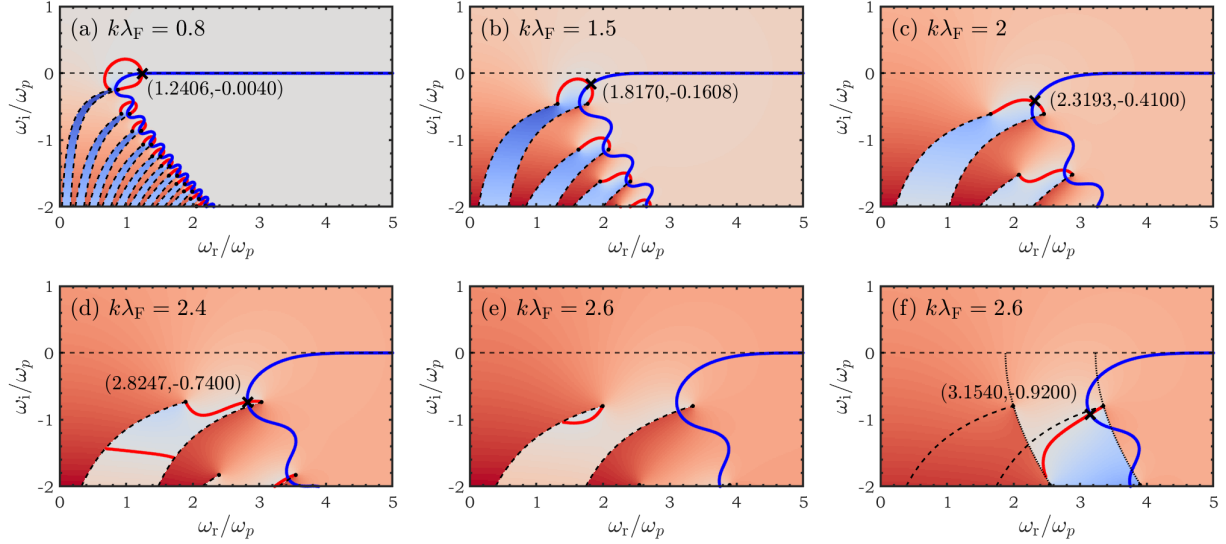


Figure 4. Complex frequency plane of dispersion function, with $\Theta = 0.2$, $\hat{h} = 0.2$.

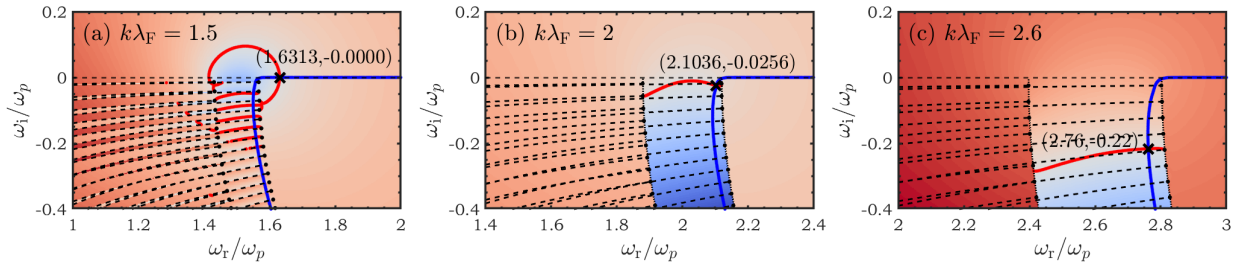


Figure 5. Complex frequency plane of dispersion function, with $\Theta = 0.006$, $\hat{h} = 0.06$.

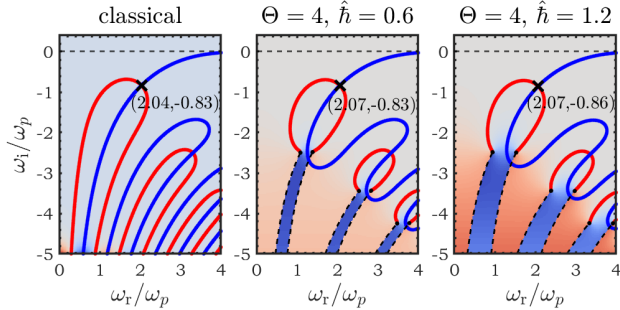


Figure 6. The DF complex frequency plane of classical and almost-classical plasmas.

corresponding to electron number density $n = 3 \times 10^{26} \text{cm}^{-3}$, and $\Theta = 0.1, 0.2$, and 0.4 , are corresponding to the temperature $T = 170, 340$ and 680eV . In both the two cases, the eigen frequency of lower temperature plasmas surpass the higher temperature when k is large enough, which is the result of the quantum topological shape. In panel (c), all the curves

are calculated with $\Theta = 0.02$, since the shape of the curves hardly change when Θ further decreases, we annotated them as $\Theta < 0.02$, or, one can simply treat them as zero-temperature results. The dashed-lines attached to each solid line are the corresponding upper bounds of the EHEC. One can see that, the solid lines are slightly lower than the dashed-lines only in a very small region, which means that the EHEC predicted by Eq. (21) is incorrect when k is large. This is because the derivation of Eq. (21) is based on the SDA, which is incorrect for finite damping rate.

C. Numerical Benchmark of the Normal Modes

The WPS, i. e., Eq. (7) and (9) can be solved numerically^{15,16} as a initial value problem. We set the initial perturbation as

$$f(x, v, 0) = [1 + A \cos(k_0 x)] f_{1d}(v), \quad (24)$$

and let it evolve, then measure the frequency and damping rate of the perturbation. The factor A is chosen to be very small to avoid nonlinear effects. When the initial perturbation is set,

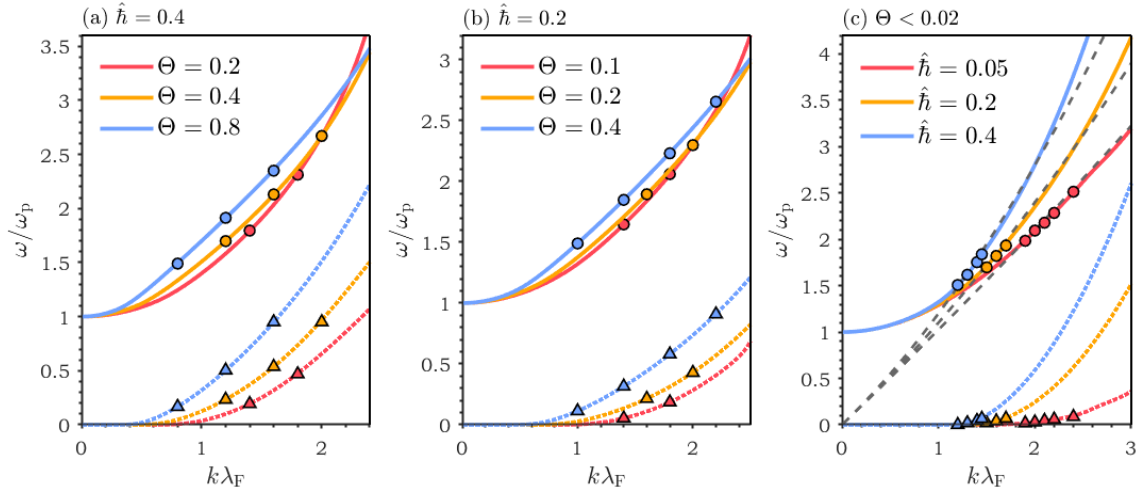


Figure 7. Dispersion relation calculated via AC method, where the solid lines stand for real frequency and dashed-lines for imaginary, and the colored markers are simulation results (square for real and triangle for imaginary part).

the time-dependent behavior of the perturbed field $\delta\phi$ consist of a ballistic mode and an infinity number of normal mode, and this can be shown by rewrite Eq. (10) as

$$\delta\phi(t, k) = \frac{1}{k^2} \int dv \delta f_{k0}(v) \times \left[\frac{e^{-ikvt}}{\varepsilon(kv, k)} + \sum_n \frac{e^{-i\omega_n t}}{(\omega_n - kv) \partial_{\omega_n} \varepsilon} \right], \quad (25)$$

where the first term in the bracket stands for the ballistic mode while the second the normal modes.

Some results are presented also in Fig. 7, where the colored circles stand for real frequency measured from simulation result, and the triangles for damping rate. The simulation results and the numerical results of normal modes match up perfectly. However, the simulation results of high- k modes are not shown, especially in panel (c), where the damping rates of the simulation points with the largest k are one order lower than they real frequency. We do not present the result of high k because it is found that those high- k modes have uncertain frequency, or, do not damp exponentially, it is impossible to measure the complex frequency nor the damping rate. The reason for this non-exponential behavior is, as we have mentioned previously, in degenerate plasmas, when k is large enough, the topological shape of the real locus become non-classical, which results in the frequency and the damping rate of normal modes increase faster than linear with k . Hence, beyond a critical value of k , the damping rate of the normal mode will surpass the ballistic mode, the time-dependent behavior then dominated by the ballistic mode. This phenomenon does not occur in a classical plasma since its dispersion relation is always linear as k increases (when $k\lambda_D \gtrsim 1$).

The proof of the above statement is represented in Fig. 8, where the red lines are the pure ballistic evolution obtained by integrate the first term in Eq. (25). In panel (a), where $\Theta = 0.2$ and $\hat{\hbar} = 0.6$, when $k = 1.3$, the ballistic mode damps faster than the normal mode, hence the simulation result shows a

clear normal mode with $\omega_i = -0.185$ (the dotted line stands for $e^{-0.185t}$). However, when $k = 2.1$, the normal mode should give $\omega_i = -0.944$, while the simulation curve damps slower than $e^{-0.944t}$ and is almost identical to the ballistic mode, and it confirms our conclusion. Also noticing that, the simulation curve does not have a clear real frequency. Similarly, in panel (b), where $\Theta = 0.02$ and $\hat{\hbar} = 0.05$, a clear normal mode with $\omega_i = -0.0957i$ is measured for $k = 2.1$, but for $k = 2.9$ the long time behavior is interfered by ballistic mode, hence no clear normal mode can be seen.

IV. DISCUSSION AND CONCLUSION

In this paper, we adopt the analytical continuation scheme to solve the dispersion relation of degenerate plasma. Compared to SDA scheme, the AC scheme can solve the normal modes of a dielectric system with arbitrarily high k , which is crucial when small-wavelength quantum kinetic effects are encountered. We find that in degenerate plasmas, the normal mode frequency and its damping rate increase with k steeper than linear, which is related to the ‘‘quantum’’ topological shape of the root locus. As a result, the temporal evolution of a high- k perturbation in quantum plasmas is dominated by ballistic mode. Especially, the exact solution of linear dispersion relation is the basis of the quantitative analysis of nonlinear effects such as parametric decay, two-plasmon decay, Raman scattering, and etc., in dense plasmas.

V. ACKNOWLEDGEMENTS

This work was supported by the Strategic Priority Research Program of Chinese Academy of Sciences (Grant No. XDA250050500), the National Natural Science Foundation of China (Grant No. 12075204), and Shanghai Municipal

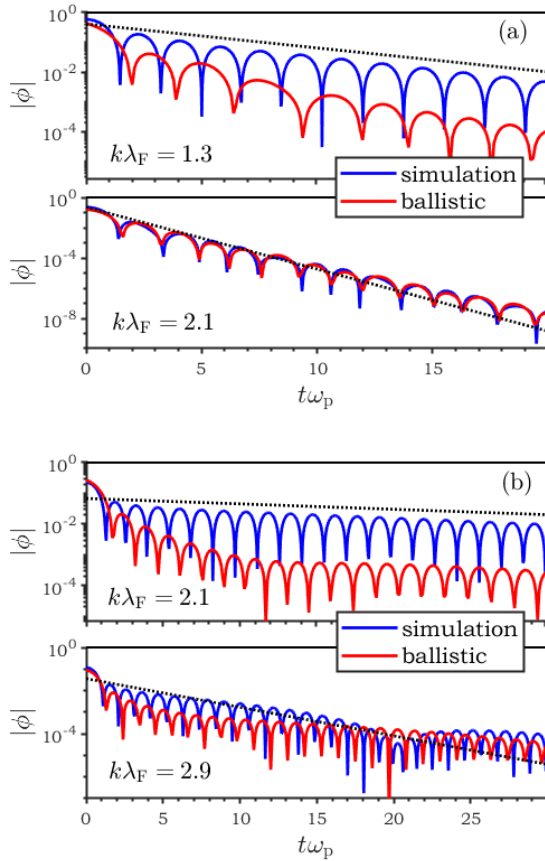


Figure 8. Temporal evolution of linear perturbations calculated by numerical simulation (the blue lines), and the ballistic evolution (the red lines): (a) $\Theta = 0.2$, $\hbar = 0.6$, (b) $\Theta = 0.02$, $\hbar = 0.05$. The dotted-lines indicate the damping rate calculated by the eigen equation (14).

Science and Technology Key Project (No. 22JC1401500). Dong Wu thanks the sponsorship from Yangyang Development Fund.

REFERENCES

- ¹Dmitri A Uzdensky and Shane Rightley. Plasma physics of extreme astrophysical environments. *Reports on Progress in Physics*, 77(3):036902, mar 2014.
- ²Giovanni Manfredi, Paul-Antoine Hervieux, and Jérôme Hurst. Phase-space modeling of solid-state plasmas: A journey from classical to quantum. *Reviews of Modern Plasma Physics*, 3(1):13, 2019.
- ³Xiaoguang Li, Di Xiao, and Zhenyu Zhang. Landau damping of quantum plasmons in metal nanostructures. *New Journal of Physics*, 15(2):023011, 2013.
- ⁴S. H. Glenzer, C. A. Back, K. G. Estabrook, R. Wallace, K. Baker, B. J. MacGowan, B. A. Hammel, R. E. Cid, and J. S. De Groot. Observation of two ion-acoustic waves in a two-species laser-produced plasma with thomson scattering. *Phys. Rev. Lett.*, 77:1496–1499, Aug 1996.
- ⁵Jie Zhang, WM Wang, XH Yang, D Wu, YY Ma, JL Jiao, Z Zhang, FY Wu, XH Yuan, YT Li, et al. Double-cone ignition scheme for inertial confinement fusion. *Philosophical transactions of the Royal Society A*, 378(2184):20200015, 2020.
- ⁶D. Wu, W. Yu, S. Fritzsche, and X. T. He. Particle-in-cell simulation method for macroscopic degenerate plasmas. *Phys. Rev. E*, 102:033312, Sep 2020.
- ⁷Xiaochuan Ning, Tianyi Liang, Dong Wu, Shujun Liu, Yangchun Liu, Tianxing Hu, Zhengmao Sheng, Jieru Ren, Bowen Jiang, Yongtao Zhao, and et al. Laser-driven proton-boron fusions: Influences of the boron state. *Laser and Particle Beams*, 2022:e8, 2022.
- ⁸Tsvi Piran. The physics of gamma-ray bursts. *Reviews of Modern Physics*, 76(4):1143, 2005.
- ⁹Frederick D Seward and Philip A Charles. *Exploring the X-ray Universe*. Cambridge University Press, 2010.
- ¹⁰Sergei V Vladimirov and Yu O Tyshetskiy. On description of a collisionless quantum plasma. *Physics-Uspekhi*, 54(12):1243, 2011.
- ¹¹Leo P Kadanoff. *Quantum statistical mechanics*. CRC Press, 2018.
- ¹²Liu Chen. *Waves and instabilities in plasmas*, volume 12. World scientific, 1987.
- ¹³Jens Lindhard. On the properties of a gas of charged particles. *Kgl. Danske Videnskab. Selskab Mat.-Fys. Medd.*, 28, 1954.
- ¹⁴Q. S. Feng, C. Y. Zheng, Z. J. Liu, L. H. Cao, Q. Wang, C. Z. Xiao, and X. T. He. Stimulated Brillouin scattering behaviors in multi-ion species plasmas in high-temperature and high-density region. *Physics of Plasmas*, 26(5):052101, 05 2019.
- ¹⁵Nam-Duk Suh, Marl R Feix, and Pierre Bertrand. Numerical simulation of the quantum liouville-poisson system. *Journal of Computational Physics*, 94(2):403–418, 1991.
- ¹⁶Tian-Xing Hu, Jiong-Hang Liang, Zheng-Mao Sheng, and Dong Wu. Kinetic investigations of nonlinear electrostatic excitations in quantum plasmas. *Physical Review E*, 105(6):065203, 2022.